The double-edged role of FASII regulator FabT in *Streptococcus pyogenes* infection

Clara Lambert[1†], Marine Gaillard[1], Paprapach Wongdontree[2], Caroline Bachmann[1], Antoine Hautcoeur[1], Karine Gloux[2], Thomas Guilbert[1], Celine Méhats[1], Bastien Prost[3], Audrey Solgadi[3], Sonia Abreu[4], Muriel Andrieu[1], Claire Poyart[1,5], Alexandra Gruss[2*] and Agnes Fouet[1*].

[1]Université Paris Cité, Institut Cochin, INSERM, U1016, CNRS, UMR8104, Paris, France;
[2]Micalis Institute, INRAE, AgroParisTech, Université Paris-Saclay, Jouy en Josas, France;
[3]UMS-IPSIT - Plateforme SAMM, Université Paris Saclay, France;
[4]Lipides: Systèmes Analytiques et Biologiques, Université Paris-Saclay, 91400 Orsay, France.
[5]AP-HP Centre–Université Paris Cité, Paris, France.

[*]email: agnes.fouet@inserm.fr ; alexandra.gruss@inrae.fr

[†] Present address: Molecular Microbiology and Structural Biochemistry, CNRS, Université de Lyon, Lyon, France

Orcid numbers: A. Fouet, 0000-0001-7715-9157; A. Gruss, 0000-0001-7426-5229; C. Lambert, 0000-0003-2740-1755; T. Guilbert, 0000-0001-5069-0730

Abstract

In *Streptococcus pyogenes*, the type II fatty acid (FA) synthesis pathway FASII is feedback-controlled by the FabT repressor bound to an acyl-Acyl carrier protein. Despite FabT defects being linked to reduced virulence in animal models, spontaneous *fabT* mutants arise *in vivo*. To resolve this paradox, we characterized the conditions and mechanisms that require FabT activity, and those that promote *fabT* mutant emergence. The primary *fabT* mutant defect is energy dissipation: specific nutrients are consumed, but the mutant fails to grow on human tissue, cells, or cell filtrates where nutrients are limited. These features explain the FabT requirement during infection. Conversely, *fabT* mutants exhibited a marked growth advantage over the wild-type in biotopes rich in saturated FAs. *fabT* mutants emerge in this context, where continued FASII activity prevented environmental FA incorporation. An *ex vivo* muscle model demonstrated that wild-type *S. pyogenes* was inhibited, while *fabT* mutant growth was stimulated, but conditional to FASII activity. Our findings elucidate the rationale for emerging *fabT* mutants that improve survival in lipid-rich biotopes, but lead to a genetic impasse for infection.

38 **Introduction**

39

40 Bacterial membranes form a mutable permeable barrier that facilitates adaptation to a changing
41 environment. They usually comprise a phospholipid bilayer composed of a polar head and
42 apolar fatty acid (FA) chains. The FA synthesis pathway (FASII), which is widespread among
43 bacteria, synthesizes saturated and/or unsaturated FAs joined to an acyl carrier protein (ACP;
44 forming acyl-ACP) (Supplementary Fig. 1a). Unsaturated FAs are produced *via* a FASII shunt
45 catalyzed by an acyl-ACP-isomerase named FabM in streptococci. While FASII is conserved
46 (with some enzyme variation), its regulators differ among Firmicutes. In streptococcaceae and
47 enterococcaccae, FASII gene expression is controlled by a unique MarR-family feedback-type
48 regulator named FabT encoded in the main FASII locus (Supplementary Fig. 1 b-c). FabT uses
49 acyl-ACP as corepressor [[1,2], for review [3]]. The affinity of FabT-(acyl-ACP) binding to a
50 specific DNA palindromic sequence increases with the length of the acyl carbon chain and the
51 presence of an unsaturation [4]. FabT regulons were characterized in various streptococcaceae
52 species and in conditions that affect membrane FA composition, including growth temperature,
53 pH or growth phase [5-9]. FabT exerts greater repression of genes encoding elongation steps,
54 mainly the *trans*-2-enoyl-ACP reductase II FabK, and less repression of *fabM*. In *Streptococcus*
55 *pneumoniae fabM* expression is not repressed by FabT [6]. Accordingly, an *S. pneumoniae* strain
56 lacking a functional FabT produced longer and more saturated FAs [6]. FabT regulons reportedly
57 also comprise non-FASII genes involved in transport, DNA and carbohydrate metabolism,
58 protein, purine and pyrimidine synthesis; however, their identities vary according to reports and
59 the species under study [3]. To date, FabT regulons were not analyzed in the presence of
60 exogeneous FAs (eFAs), which enhance FabT transcriptional repression [4]. This missing
61 information is particularly relevant as numerous host infection sites are FA-rich.

62 *Streptococcus pyogenes*, also known as Group A *Streptococcus*, GAS, is a major human
63 pathogen causing mainly extracellular infections, which is responsible for a large variety of
64 clinical manifestations ranging from superficial infections to life-threatening invasive
65 infections [10]. GAS infections rank among the top ten causes of death due to bacterial infections
66 worldwide [11]. GAS isolates mutated in *fabT* were recovered in non-human primates at the point
67 of intramuscular inoculation, raising the possibility of such populations forming in the human
68 host [5]. In a murine model, strains harboring *fabT* point mutations display smaller size lesions,
69 no loss of body weight and a lower mortality than their wild-type counterparts [12]. In a non-
70 human primate model, a *fabT* deleted strain shows decreased colonization and dissemination
71 capacities compared to the parental strain [5]. Its survival is also decreased in human blood or in
72 the presence of human polymorphonuclear leukocytes [5].

73 These reported properties indicate that the *fabT* mutant variants are poorly adapted for
74 infection, which led us to question the rationale for their emergence. We solve this question
75 here by performing in-depth analyses of the features of WT and a representative *fabT* mutant
76 in different conditions relevant to host infection. We report that the *fabT* mutant is metabolically
77 wasteful, by consuming sugars and amino acids, yet failing to grow, which accounts for its
78 failure to cause infection. Conversely, saturated FA-rich environments impose a counter-
79 selective pressure against WT bacteria expressing active FabT. We show that *fabT* mutant
80 growth is stimulated around lipid-rich muscle sources in a FASII-dependent manner, while WT
81 growth is inhibited. These findings solve the apparent contradiction between the *in vivo*
82 emergence of attenuated *fabT* variants and the need for an active FabT repressor during
83 infection.

84 **Results**

85

86 **WT and *fabT* mutant growth properties**

87 Multiple independent FabT point mutants were harvested from the infection site of nonhuman
88 primates, some of which mapped to His105 [5]. We chose the FabT^{H105Y} point mutation as being
89 representative of mutations that arose *in vivo*, which was established in the *emm28* reference
90 strain M28PF1 (respectively mFabT and WT) [13,14] (Supplementary Fig. 1b-c) [15]. A Δ*fabT*
91 deletion strain was constructed for phenotypic comparisons (Supplementary Fig. 2). mFabT
92 and WT strains grow similarly in laboratory medium (THY), and in THY supplemented with
93 0.1 % Tween 80 (THY-Tween, a C18:1Δ9 [oleic acid] source) (Supplementary Fig. 2a-b, left;
94 also see [2]). Survival of WT and mFabT strains in mid-exponential phase was also comparable,
95 as assessed by live-dead staining (Supplementary Fig. 2a-b, right). Unlike mFabT, the Δ*fabT*
96 mutant grew slowly in both THY and THY-Tween media (Supplementary Fig. 2c-d; also see
97 [12]). As *fabT* deletions were not reported to arise *in vivo,* we chose to study the mFabT mutant
98 strain as being representative of *in vivo* mutations.

99

100 **FabT^{H105Y} impacts membrane lipid production and species**

101 The GAS mFabT strain produced greater proportions of longer length saturated FA (C18:0)
102 than the WT strain (26.1 % *versus* 6.8 % respectively; Supplementary Table 1), as first reported
103 in *S. pneumoniae* [6]. In THY-Tween, which supplies C18:1Δ9, the native FabT represses FASII,
104 and contains 1.7 times more C18:1Δ9 than does mFabT. In this condition, the proportion of
105 C18:0 remained higher in mFabT than in the WT (12.4 % and 0.2 % respectively;
106 Supplementary Table 1) [2]. For comparison, the Δ*fabT* mutant showed a higher C18:0 to C16:0
107 ratio than mFabT in both THY and THY-Tween, likely reflecting complete FASII derepression

108 in the deletion strain (Supplementary Table 1). The more extreme membrane FA differences
109 may account for poor Δ*fabT* growth in laboratory media.

110 The effects of the FabT mutation on membrane FA composition should also alter
111 phospholipid metabolism. Lipid analyses of WT and mFabT strains cultured in THY and THY-
112 Tween media identified notable differences in membrane lipid features: i, the primary
113 differences between WT and mFabT FA composition were reflected in the identifiable lipid
114 species **(**Supplementary Fig. 3, Supplementary Table 2)**;** ii, THY grown mFabT has ~60 %
115 overall lipid yield compared to that of the WT, extracted from equivalent bacterial OD_{600} (N=4);
116 these differences were narrowed to ~5 % in cultures grown in THY-Tween (Supplementary
117 Table 3). We cannot explain these differences in yield, but suggest that the different FA
118 composition of mFabT might affect extraction efficiency. The reasons for these differences in
119 yield will require further study. Among the detected lipids, diglucosyldiacylglycerol (DGDG)
120 and cardiolipin (CL) amounts were proportionately lower in mFabT compared to WT in THY
121 medium. In THY Tween, levels of both CL and DGDG decreased for WT, but not for mFabT
122 (Fig. 1a-b). iii, CL species in mFabT were 2-fold enriched in deoxidized cardiolipin (deoxy-
123 CL) species compared to CL in the WT strain, regardless of the growth medium (Fig. 1c-e). CL
124 but not deoxy-CL reportedly facilitates oxidative phosphorylation activity by binding protons
125 [16]. In conclusion, the greater proportions of saturated and longer FAs in the *fabT* mutant appear
126 to cause a reduced overall membrane lipid content and alterations in lipid distribution and
127 composition as compared to the WT.

128 *fabT* mutants are reportedly more resistant to the cationic cyclic peptide polymyxin B
129 [5,17]. Polymyxin B binds negatively charged lipids such as CL [18]. Putting together these reports
130 and the CL changes noted above, we examined polymyxin B resistance of mFabT and WT
131 strains in conditions where CL amounts varied (Fig. 1f). Features that decreased CL pools, *i.e.*,
132 *fabT* mutation or FA availability during WT growth, correlated with greater polymyxin B

133 resistance. These data support the idea that greater polymyxin B resistance in *fabT* mutants is
134 due to lower CL pools, and show that availability of environmental FAs can lead to polymyxin
135 B resistance. They give a rationale for *fabT* mutant emergence upon polymyxin B selection [17].
136 However, they do not explain the *in vivo* emergence of mFabT mutants at an early stage of GAS
137 infection.
138
139 **Effects of *fabT* on FASII and virulence factor expression**
140 We first examined the basis for the shift towards greater amounts of C18:0 in the mFabT strain
141 when grown in THY medium (Supplementary Table 1). In THY-Tween, FASII genes are
142 repressed in WT, but not detectably in mFabT [2]. In FA-free THY medium however, the only
143 difference in *S. pyogenes* FASII gene expression was a greater expression of *fabK* in mFabT
144 than in the WT strain, leading to an increased *fabK*: *fabM* ratio in the mFabT mutant, as reported
145 for a *fabT* mutant in *S. pneumoniae* ([2,6]; Supplementary Fig. 4a). FabK and FabM compete for
146 the same substrate to respectively synthesize saturated and unsaturated FAs (Supplementary
147 Fig. 1a); thus, higher *fabK* expression relative to *fabM* is consistent with the higher proportion
148 of saturated FAs in *fabT* mutants [2,6]. The underlying reason for a higher *fabK*:*fabM* ratio in the
149 mFabT mutant was revealed by analyzing FASII locus organization by qRT-PCR
150 (Supplementary Fig. 4b). All genes from *fabM* to *accD* were cotranscribed. In addition,
151 transcription start sites are present within this operon (Fig. 2a) [19]. All transcriptional start sites
152 except that of *fabH* are preceded by FabT consensus DNA binding motifs (5'-
153 ANTTTGATTATCAAATT). Notably, two FabT binding sites are predicted upstream of *fabK*,
154 but not of the other FASII transcriptional units (starting positions 400693 and 400931 on the
155 *emm28* M28PF1 genome [CP011535.2] [13]) [3]. We suggest that the double FabT binding sites
156 upstream of *fabK*, and basal levels of free FAs in THY are responsible for differential *fabK*
157 *fabM* regulation and hence increased saturated FA synthesis in the mFabT mutant.

158 We then used RNAseq and qRT-PCR to identify how membrane FA changes might
159 impact and explain the virulence defect during host infection. WT and mFabT expression was
160 compared in THY, and in THY-Tween (as C18:1Δ9 source) to activate WT FabT repression ([3]
161 for Review; Supplementary Table 4, Fig 2b-e, Supplementary Figure 4c). Several differences,
162 some corresponding to multi-gene operons, distinguished the two strains (Supplementary Table
163 4). Notably, purine synthesis operon genes (M28_Spy0022 to M28_Spy0026) were upregulated
164 in mFabT, suggestive of increased metabolic activity. An operon encoding adhesins
165 (M28_Spy0107 to M28_Spy0111) was also upregulated; however, expression of virulence
166 genes of the Mga regulon, i.e., C5 peptidase ScpA, and other adhesins, M protein, Sof and
167 SfbX, were down-regulated (Supplementary Table 4). Decreased expression of adhesins and
168 other virulence factors such as SLO (*slo*) and NADase (*nga*) could contribute to the reported
169 poor virulence of *fabT* mutants in infection [20].

170 Addition of C18:1Δ9 activates FabT-mediated repression, which, as reported, turns off
171 FASII gene expression in the WT strain (Fig. 2c, Supplementary Table 4) [4]**.** In contrast, FASII
172 genes (see above), and a non-FASII gene within the FabT regulon (M28_Spy1638, encoding a
173 putative fatty acid kinase binding protein; [14]), remain transcriptionally active in the mFabT
174 mutant, showing that $FabT^{H105Y}$ is defective for FASII repression (Fig. 2e, Supplementary
175 Table 4).

176 Despite the more pronounced difference in FASII gene expression between WT and
177 mFabT in THY-Tween, only few differences were observed in virulence gene expression. We
178 noted that virulence genes lack FabT binding motifs, suggesting an indirect effect of FabT on
179 their expression. Of note, in THY medium, the mFabT mutation led to longer chain lengths
180 than in WT (determined as C18 to C16 ratios of respectively 2.3 and 1; Supplementary Table
181 1). In THY-Tween, these ratios are comparable; the WT C18:C16 ratio increased to 2. We
182 speculate that the higher C18:C16 ratio of membrane FAs may provoke lower virulence gene

183 expression, as seen for mFabT in THY, and the WT in THY-Tween (Supplementary Table 4).
184 Thus, the greater proportion of longer FAs in the membrane might be a cause for the decreased
185 expression of virulence genes that lack FabT binding motifs.
186

187 **The WT strain has a fitness advantage over mFabT during growth on human decidua**

188 To understand the role of *fabT* and emergence of *fabT* mutants, we designed *ex vivo* assays to
189 study infection with WT and *fabT* variants. mFabT strain capacity to colonize human tissue *ex*
190 *vivo* was assessed by measuring its growth on human tissue. As *emm28* strains are associated
191 to puerperal fever [21,22], we compared *ex vivo* growth of WT and mFabT on human decidua [23].
192 In control experiments, both strains failed to grow in RPMI, as assessed by growth ratios
193 between cfus after 8 h incubation and the inocula (Supplementary Fig. 2e). In static conditions,
194 growth of mFabT was 63 % lower than that of the WT strain (Fig. 3a). Growth kinetics of
195 WT$^{eryR\text{-}igfp}$ and mFabT$^{eryR\text{-}igfp}$ GFP-marked strains were then followed in flow conditions at the
196 tissue surface by time-lapse microscopy (Fig. 3b-c). The surface colonized by the WT strain
197 increased throughout the 4 h growth period (Fig. 3b). In contrast, mFabT strain growth only
198 increased during the first half-hour of image acquisition. The average thickness of bacterial
199 microcolonies increased for the WT, but decreased for the mFabT strain (Fig. 3c). Altogether,
200 the WT strain grew with a doubling time of roughly 200 min whereas the mFabT strain did not
201 grow. Thus, in contrast to normal growth in THY medium, the mFabT strain has a major growth
202 defect in the presence of human decidua. These results provide insight into the nature of the
203 colonization defect and virulence attenuation of *fabT* mutant strains [5,12].
204

205 **Impaired mFabT fitness is due to defective adhesion and poor growth on human cells and**
206 **in cell supernatants**

207 Bacterial colonization of host tissue comprises an initial adhesion step, followed by bacterial
208 multiplication [23]. As GAS has tropism for endometrial and skin tissues, we compared WT and
209 mFabT adhesion capacities on human endometrial cells, and on differentiated (as present in
210 upper skin layers), and undifferentiated skin keratinocytes (Fig. 3d). The mFabT mutant
211 displayed an adhesion defect on endometrial cells as reported [2] and undifferentiated
212 keratinocytes compared to the WT. In contrast, the strains adhered similarly on differentiated
213 keratinocytes. The adhesion defect, as also suggested by transcriptome analyses
214 (Supplementary Table 4, Fig. 3d), may contribute to the virulence defect observed in the non-
215 human primate animal models [5].

216 GAS replicates mainly extracellularly during infection of endometrium and skin [24].
217 Growth comparisons of WT and mFabT strains on these biotopes, namely endometrial cells,
218 undifferentiated keratinocytes, and differentiated keratinocytes, showed that the mFabT strain
219 was decreased (90 %, 53 % and 56 % respectively) compared to the WT strain (Fig. 3e). The
220 $FabT^{H105Y}$ mutation thus leads to impaired growth in the presence of human cells. To determine
221 whether adhesion is required for the growth differences between WT and *fabT* strains, we
222 assayed bacterial growth in uninfected cell supernatant, termed "conditioned supernatant" (Fig.
223 3f). The mFabT strain displayed a similar growth defect in endometrial, undifferentiated and
224 differentiated keratinocyte conditioned supernatants (72 %, 50 % and 50 % respectively)
225 compared to the WT. This indicates that cell-secreted products differentially affect growth of
226 WT and mFabT strains. Adhesins differentially produced in WT (Supplementary Table 4, Fig.
227 3d) could also contribute to promoting higher bacterial densities during infection.

228 The differences in WT and mFabT growth were visible when grown on endometrial cells
229 or their conditioned supernatants. It is therefore likely that secreted endometrial cell compounds
230 affecting GAS growth are produced independently of infection. Higher bacterial growth
231 densities on differentiated keratinocytes than on conditioned supernatants (compare Fig. 3e and

232 3f) may be due to greater nutrient availability after infection. Altogether, these data implicate
233 both adhesion and growth defects in poor survival of mFabT in cell infection environments.
234 Poor mFabT growth suggests that mFabT makes inefficient use of nutrients secreted by
235 eukaryotic cells and/or is more susceptible than WT to secreted bactericidal molecules. We
236 investigated growth kinetics of WT and mFabT strains in endometrial cell conditioned
237 supernatant in time course experiments (Fig. 3g left). Cfu ratios were similar for both strains at
238 4 h, indicating no difference in the lag time. However, from 8 h onwards, cfu ratios were higher
239 for the WT strain (Fig. 3 f,g left). The use of a live-cell analysis (IncuCyte® Systems, Sartorius,
240 Germany), in which both living and dead bacteria are visualized, revealed that mFabT growth
241 did not peak before the WT, and that both strains grew similarly until ~3 h; after 3 h mFabT net
242 growth is visibly slower than that of the WT strain (Supplementary Fig. 2f). mFabT mortality
243 was ~1.5-fold greater than WT at 8 h post-inoculation in conditioned supernatant (Fig. 3g right);
244 these differences are amplified at 16 h and 24 h (Fig. 3g left). We noted that GAS dies rapidly
245 when growth stops, as seen in RPMI (Supplementary Fig. 2e). We conclude that mFabT grows
246 more slowly and dies more rapidly than the WT strain, and lead us to suggest that mFabT death
247 is triggered by poor growth on nutrient-limited medium.
248
249 **Faster metabolic turnover in mFabT generates a growth defect during infection**
250 We investigated a possible metabolic basis for the mFabT growth defect, which could reflect
251 an incapacity to use cell-secreted products for growth, and/or higher mortality (Fig. 3g). We
252 used a metabolomics approach to assess metabolites that are differentially consumed by mFabT
253 compared to the WT strain, as performed on conditioned supernatants. Hexoses and amino
254 acids, Asn, Gly, Ile and Lys were the main metabolites overproduced by uninfected cells
255 (Supplementary Fig. 5, Supplementary Table 5). The mFabT strain consumed more hexoses
256 and amino acids Asn, Ile, Lys, and Ser, as seen at 16 h (Fig. 4, Supplementary Table 5). This

257 overconsumption is not linked to a higher bacterial yield, but rather the opposite. It is also not
258 due to faster growth of the mutant relative to WT, but rather to a lower bacterial yield resulting
259 from accrued mortality of this strain (Fig 3g, Supplementary Fig. 2f).

260 Two characteristics of mFabT may underlie this futile cycle: 1- The high C18:C16 ratio
261 in mFabT compared to WT (respectively 2.3 to 1; Supplementary Table 4) may reduce bacterial
262 fitness by altering activities of membrane components, leading to greater mortality in nutrient-
263 limited medium. 2- Lipid synthesis and FA availability reportedly play a role in regulating
264 metabolic functions [25]. Continued FASII expression in mFabT may desynchronize coordination
265 between membrane synthesis and growth, such that metabolite import remains active even if
266 other growth factors are unavailable. Consistently, increased mFabT metabolite consumption
267 and greater mortality occurred after 8 h incubation, when growth presumably slows (Fig. 3g,
268 Fig. 4). These data give evidence that the mFabT mutant has greater metabolic consumption at
269 the GAS site of infection, but without growth benefits. Futile energy loss in mFabT might be
270 further due to expression changes associated with its altered membrane FA composition and
271 continued FASII synthesis, leading to increased mortality in nutrient-limited biotopes. These
272 factors might account for the diminished capacity of *fabT* mutants to cause infection [5].

273

274 **Continued FASII activity in the mFabT mutant leads to lower eFA incorporation.**

275 C18:1Δ9 incorporation is reduced in the mFabT strain (Supplementary Table 1). In *S.*
276 *pneumoniae*, a *fabT* mutant reportedly incorporated only traces of C16:1 [6]; in an *Enterococcus*
277 *faecalis fabT* deletion mutant, incorporation of unsaturated FAs, and to a lesser extent, saturated
278 FAs, was defective [4]. We evaluated FA incorporation by GAS in medium supplemented with
279 C17:1, which is not synthesized by GAS; incorporation of this FA generates a discrete peak by
280 gas chromatography (Fig. 5a left). The proportion of C17:1 was 3-fold higher in the WT than
281 in mFabT (52 %:17 %).

282 Continued FASII synthesis in the mFabT mutant might create competition between
283 endogenously synthesized FAs and eFAs for incorporation into membrane phospholipids. To
284 test this, we performed the same experiments in the presence of platensimycin (Fig. 5a right),
285 a FabF inhibitor that blocks FASII synthesis independently of FabT [26]. WT and mFabT strains
286 grew similarly in the presence of C17:1 and platensimycin (Supplementary Table 6), and C17:1
287 was the major membrane FA in both strains (Fig. 5a). In conclusion, the $FabT^{H105Y}$ mutant is
288 less responsive to environmental FAs than the WT strain. Poor eFA incorporation in mFabT
289 phospholipids thus correlates with continued expression of FASII genes.
290

291 ***De novo* emergence of *fabT* mutants in saturated FA environments**

292 We hypothesized that the defect in eFA incorporation could actually confer a growth advantage
293 to the mFabT strain in toxic lipid environments, and thereby point to conditions of *fabT* mutant
294 emergence. Indeed, FA incorporation can negatively affect bacterial integrity, and free FAs are
295 considered part of the first line of host defense against skin infections [27]. Notably, increased
296 C18:0 levels in the mFabT mutant compared to WT ([2]; Supplementary Table 1) led us to
297 examine saturated FAs as potential selective pressure for *fabT* emergence. WT and mFabT
298 growth and eFA incorporation were then compared in the presence of C14:0 and C16:0, both
299 of which are found among host lipids [28]. Both FAs inhibited WT growth, and were nonetheless
300 efficiently incorporated in WT membranes; in striking contrast, mFabT failed to incorporate
301 C14:0, and incorporated >2-fold less C16:0, while strain growth was robust (Fig. 5b-c). This
302 growth advantage incited us to consider that spontaneous *fabT* mutants could emerge in the
303 presence of saturated FAs.

304 As proof of concept, we grew the WT strain in THY liquid medium without or with
305 C14:0, and then streaked cultures on solid medium containing C14:0. Single colonies appeared
306 on this medium, and *fabT* genes were sequenced. Mutations in *fabT* were obtained in both

307 selection procedures, and encoded FabT variants FabT^{T65M} and FabT^{G99S} (Supplementary Fig.
308 1b-c). Both these variants were also identified in a primate infection study [5]. We compared
309 growth and FA-incorporation phenotypes of the isolated FabT^{T65M} and FabT^{G99S} mutants, as
310 well as Δ*fabT* mutant as reference, to those of WT and mFabT strains Supplementary Fig. 6.
311 Growth at 4h of the newly isolated mutants, mFabT and Δ*fabT*, was essentially unaffected by
312 C14:0. Moreover, the mutant expressing FabT^{T65M}, mFabT and Δ*fabT* strains incorporated ≤
313 2 % C14:0 compared to ~53 % ± 6 in the WT. The mutant expressing FabT^{G99S} incorporated
314 20 % ± 3, well below that in the WT strain. These results provide a rationale for emergence of
315 *fabT* mutants, by generating a growth advantage in lipid-containing biotopes as may be present
316 at the infection locus.
317

318 **Evidence that eFA exclusion by mFabT confers a growth advantage in a simulated muscle**
319 **biotope**

320 We hypothesized that *fabT* mutations could provide a transient advantage in lipid-rich biotopes,
321 which would explain their emergence in muscle [5]. An *ex vivo* model was devised to assess
322 effects of muscle on GAS growth. For this, commercial organic 15 % fat meat, *i.e.*, muscle
323 from cattle, was placed on lawns of WT$^{eryR\text{-}igfp}$ and mFabT$^{eryR\text{-}igfp}$. This is within the percent fat
324 range estimated for human muscle (8-30 %; in contrast, uterine fluid lipid concentrations are
325 >1000-fold lower [29,30]). Remarkably, WT strains developed a weak inhibitory halo surrounding
326 the muscle samples. In strong contrast, the mFabT strain grew directly and vigorously around
327 muscle sources (Fig. 5d).

328 This result is consistent with growth inhibition of WT but not mFabT GAS, notably by
329 saturated eFAs (Fig. 5b). To confirm that vigorous growth of mFabT around muscle relates to
330 its lower incorporation of FAs from muscle lipids, we tested the effects of adding the FASII
331 inhibitor platensimycin to growth medium and plates. All media contained C17:1, which is

332 incorporated and allows mFabT growth in the presence of the FASII inhibitor (Fig. 5a,
333 Supplementary Table 6). As in Fig. 5d, mFabT growth was robust around muscle sources in the
334 absence of FASII inhibitor (Fig. 5e upper). In contrast, growth was strongly inhibited around
335 the muscle source when platensimycin was present (Fig. 5e lower). The marked inhibitory
336 effect of the muscle sample on the *fabT* mutant when FASII is blocked gives strong evidence
337 that incorporation of muscle lipids negatively affects GAS growth. We note that indirect effects,
338 consequent to FASII inhibition by platensimycin and/or by FabT repression, may contribute to
339 growth inhibition. We conclude that continued FASII activity in mFabT mutants reduces eFA
340 incorporation and thus protects bacteria from toxicity of host lipids as present in muscle
341 biotopes.
342
343 **Discussion**
344 Our work establishes the causal origin for *fabT* mutation emergence and provides an
345 explanation for its disappearance during invasion (Fig. 6): GAS is genetically designed to
346 incorporate eFA from lipid-containing environments, and repress FASII. We showed that WT
347 GAS growth is inhibited by saturated FAs in such environments. Counter-selection can lead to
348 emergence and outgrowth of *fabT* mutants, which explains their detection at a non-invasive
349 step of infection [5]. At this step, the *fabT* mutation would confer a transient advantage over non-
350 mutant strains. We first showed the *fabT* growth advantage, and mutant emergence, using C14:0
351 selection. We then demonstrated that the lipid-rich inter-muscular environment allows *fabT*
352 mutant growth in a FASII-dependent manner, while inhibiting the WT strain. While the overall
353 muscle and uterine fluids environments where GAS multiply are very different, it is notable
354 that their lipid concentrations, differ by ~1000-fold (150 mg/g muscle, compared to 20-200
355 µg/ml in uterine fluid [29,30]). We suggest that exposure to high inter-muscular lipid availability
356 would contribute to WT mortality. However, the *fabT* mutation has a cost for virulence: it

357 results in a multiplication defect and higher mortality in the presence of human cells, which is
358 confirmed on human decidua tissue and its fluids. Continued FASII activity in *fabT* mutant
359 strains provokes a state of futile bacterial metabolism where increased metabolite uptake does
360 not lead to improved growth.

361 Our findings indicate that futile FASII synthesis by mFabT is detrimental for GAS
362 virulence. We showed previously that blocking FASII with antibiotic inhibitors, mutation, or
363 deletion did not prevent infection by *Streptococcus agalactiae*, nor by other Firmicute
364 pathogens [31-33]. FASII inhibition and eFA incorporation in phospholipids corresponds to the
365 natural feedback inhibition in response to eFAs [3,31]. The contrary, *i.e.*, making FASII synthesis
366 constitutive by inhibiting FabT, is detrimental for *in vivo* infection. FabT is thus a promising
367 target for new therapeutics against specific Gram-positive pathogens including GAS, *S.*
368 *agalactiae*, *S. pneumoniae*, and *E. faecalis*.
369

370 **Methods**

371 **Bacterial strains and culture conditions**

372 The strains used in this study are described in Supplementary Table 7. GAS strains were grown
373 under static condition at 37 °C in Todd Hewitt broth supplemented with 0.2 % Yeast Extract
374 (THY) or on THY agar (THYA) plates, or in brain heart infusion (BHI) liquid or agar medium
375 when specified. Medium was supplemented with 0.1 % Tween 80 (THY-Tween; Sigma-
376 Aldrich, Ref. P1754) as indicated, as a source of C18:1Δ9. THY was also supplemented with
377 the saturated FAs, C14:0 and C16:0, or the unsaturated FA C17:1 (Larodan, Sweden) in the
378 presence of FA-free bovine serum albumin (0.025 %, Sigma-Aldrich, Ref. A6003) The FASII
379 inhibitor platensimycin (Tebubio, France) was added at (0.5 to 1 µg/ml) as indicated. For
380 WT$^{eryR\text{-}igfp}$ and mFabT$^{eryR\text{-}igfp}$ (Supplementary Table 7) strains, medium was supplemented with
381 5 to 10 µg/ml of erythromycin (Ery). Strains were prepared as follows, unless specified
382 otherwise: overnight cultures were diluted to an OD_{600} = 0.05 and grown in THY to the
383 exponential phase (OD_{600} comprised between 0.4 and 0.5). For GFP expression, exponential-
384 phase bacteria were further diluted to OD_{600} = 0.1 in THY supplemented with 10 µg/ml
385 erythromycin, and 20 ng/ml anhydrotetracycline to induce GFP expression, grown for 90 min
386 at 37 °C, and diluted in RPMI as indicated below. For growth in saturated FAs, WT and mFabT
387 THY precultures were diluted in THY or THY-C14:0 or THY-C16:0 to OD_{600} = 0.05,
388 transferred to 50 mL falcon tubes, and incubated at 37 °C. Growth was determined by OD_{600}
389 readings at designated time points.

390

391 **Strain constructions**

392 Primers used for cloning and strain verification are described in Supplementary Table 8. The
393 Δ*fabT* strain corresponds to a *fabT* deleted mutant. It was obtained by homologous
394 recombination of the plasmid pG1-Δ*fabT* following a published protocol [34,35]. The DNA

395 fragments encompassing *fabT* were cloned in BamHI – EcoRI digested pG1 using the In Fusion
396 cloning kit® (Clonetech). This led to the deletion of *fabT* from nucleotides 49 to 389, as
397 confirmed by PCR. The mFabT$^{eryR\text{-}igfp}$ strain harboring an integrated inducible *gfp* gene was
398 constructed as described for the WT$^{eryR\text{-}igfp}$ strain [23]. Whole genome sequencing was performed
399 on the mFabT and mFabT$^{eryR\text{-}igfp}$ constructed strains, and no surreptitious mutations were found
400 (Bioproject PRJNA926803, accession number SAMN34247893 for mFabT, SAMN34247911
401 for mFabT$^{eryR\text{-}igfp}$).
402
403 **Fatty acid analysis**
404 Strains were grown until OD_{600} = 0.4 - 0.5. Fatty acids were extracted and analyzed as described
405 [2,14,31-33]. Briefly, analyses were performed in a split-splitless injection mode on an AutoSystem
406 XL Gas Chromatograph (Perkin-Elmer) equipped with a ZB-Wax capillary column (30 m x
407 0.25 mm x 0.25 mm; Phenomenex, France). Data were recorded and analyzed by TotalChrom
408 Workstation (Perkin-Elmer). FA peaks were detected between 12 and 40 min of elution, and
409 identified by comparing to retention times of purified esterified FA standards (Mixture ME100,
410 Larodan, Sweden). Results are shown as percent of the specific FA compared to total peak areas
411 (TotalChrom Workstation; Perkin Elmer).
412
413 **Lipid analysis**
414 Strains were grown as 200 ml cultures in THY or THY-Tween until OD_{600} = 0.4 - 0.5. Lipid
415 extractions and identifications were performed as described [32,36-38]. Lipid separation was
416 realized by normal phase HPLC (U3000 ThermoFisher Scientific) using a Inertsil Si 5µm
417 column (150 x 2.1 mm I.D.) from GL Sciences Inc (Tokyo, Japan). Lipids were quantified
418 using a Corona-CAD Ultra and identified by mass-spectrometry negative ionization and
419 MS^2/MS^3 fragmentations (LTQ-Orbitrap Velos Pro). The adducts observed for molecular ions

420 were: CH3COO- for MGDG, CH3COO- and H- for DGDG, H- for PG and CL. The
421 concentration of each lipid class was determined as described using as standards (from Avanti,
422 Germany) DGDG, 840524P-5MG; MGDG, 840523P-5MG; CL (heart CA), 840012P-25MG;
423 PG (egg), 841138P-25MG [39]. Lipid spectra were analyzed on Xcalibur™ software
424 (ThermoFisher Scientific, version 4.2.47). Lipid concentrations are presented as milligrams
425 per OD_{600} = 100 for all samples. The Lipid Maps 'Structure search' program
426 https://www.lipidmaps.org/resources/tools/bulk-structure-
427 search/create?database=COMP_DB was used to identify FA moieties on identified lipid
428 species.
429
430 **Polymyxin B assay**
431 Polymyxin B sensitivity was assayed as described [5]. Bacteria were grown to OD_{600} = 0.4 - 0.5
432 in THY or THY-Tween. Serial dilutions were prepared in PBS, and 2.5 µl of each dilution was
433 inoculated onto THY or THY-Tween plates containing or not 20 $\mu g.ml^{-1}$ polymyxin B (Sigma-
434 Aldrich, Ref. 81271). Plates were incubated at 37 °C for approximately 24 h and photographed.
435 Experiments were done in biological triplicates.
436
437 **In silico analysis**
438 Geneious prime Biomatters development, www.geneious.com was used to identify 5'-
439 ANTTTGATTATCAAATT-3', the putative FabT binding sequence, on the M28PF1 genome,
440 accepting up to 2 mismatches.
441
442 **RNA isolation and Illumina RNA-seq sequencing**
443 GAS strains were cultured at 37 °C in THY or THY-Tween, and cells were harvested during
444 exponential growth (OD_{600} between 0.4 and 0.5). Independent triplicate cultures were prepared

445 for each condition. For RNA preparation, 2 volumes of RNA protect* (Qiagen) was added to
446 cultures prior centrifugation (10 min 12,000 g) and total RNA was extracted after lysing
447 bacteria by a 30 min 15 $mg.ml^{-1}$ lysozyme, 300 $U.ml^{-1}$ mutanolysin treatment at 20 °C followed
448 by two cycles of Fast-prep (power 6, 30 s) at 4 °C. RNA extraction (Macherey-Nagel RNA
449 extraction kit; Germany) was done according to supplier instructions. RNA integrity was
450 analyzed using an Agilent Bioanalyzer (Agilent Biotechnologies, Ca., USA). 23S and 16S
451 rRNA were depleted from the samples using the MICROBExpress Bacterial mRNA enrichment
452 kit (Invitrogen, France); depletion was controlled on Agilent Bioanalyzer (Agilent
453 Biotechnologies). Libraries were prepared using an Illumina TS kit. Libraries were sequenced
454 generating 10,000,000 to 20,000,000 75-bp-long reads per sample.
455
456 **RNA-Seq data analysis**
457 The MGAS6180 strain sequence (NCBI), which is nearly identical to M28PF1 [13,21], was used
458 as a reference sequence to map sequencing reads using the STAR software (2.5.2b)
459 BIOCONDA (Anaconda Inc). RNA-seq data were analyzed using the *hclust* function and a
460 principal component analysis in R 3.5.1 (version 2018-07-02). For differential expression
461 analysis, normalization and statistical analyses were performed using the SARTools package
462 and DESeq2 [40,41] *p*-values were calculated and adjusted for multiple testing using the false
463 discovery rate controlling procedure [42]. We used UpsetR to visualize set intersections in a
464 matrix layout comprising the mFabT *versus* the WT strain grown in THY and in THY-Tween,
465 and growth in THY-Tween *versus* THY for each strain [43,44]. Transcriptomic data was deposited
466 in the Mendeley database https://data.mendeley.com/datasets/68bhhsy2p4/1.
467
468 ***Ex vivo* GAS growth capacity analysis**

469 Human placentas with attached maternal-fetal membranes were collected and processed as
470 described [23] with the following modifications. Tissues were obtained after vaginal delivery, and
471 the samples used were from regions located far from the cervix, known as zone of intact
472 morphology [45]. Human decidual explants were infected within hours of their reception.

473 *Ex vivo* bacterial growth capacity in the presence of decidua human tissue was done as
474 follows: exponentially growing GFP-expressing bacteria were washed twice in PBS and diluted
475 in RPMI at a final concentration of 10^4 bacteria per ml. Decidua tissue were washed twice in
476 PBS. One ml of bacteria were then added to tissue, followed by incubation at 37 °C + 5 % CO_2.
477 After 8 h, the tissues were shredded using Precellys Evolution (Bertin Technologies) (6 x 20 s
478 at 5500 rpm with a 20 s pause between shaking). Serial dilutions of shredded material were
479 plated on THYA plates. The number of cfus was determined after 24 h of growth at 37 °C and
480 normalized to the inoculum for each experiment.

481 Live bacterial multiplication on human tissue: infection of maternal-fetal explants, image
482 acquisition and treatments were realized as described [23].

483

484 **Study approval**

485 The study of the human maternal-fetal membranes was approved by the local ethics committee
486 (Comité de Protection des Personnes Ile de France III, no. Am5724-1-COL2991, 05/02/2013).
487 All participants provided written informed consent prior to inclusion in the study at the
488 Department of Obstetrics, Port Royal Maternity, Cochin University Hospital, Paris, France.

489

490 **Cell culture**

491 HEC-1-A (ATCC_ HTB-112TM) endometrial epithelial cells were cultured as described [46], in
492 McCoy's 5A medium (Gibco, Ref. 26600080) supplemented with 10 % fetal bovine serum at
493 37 °C, 5 % of CO_2. HaCaT (Addex-Bio T0020001) keratinocytes were cultivated as

494 recommended, in DMEM high glucose medium (Gibco, Ref. 31966) supplemented with 10 %
495 fetal bovine serum at 37 °C, 5 % of CO_2. HaCaT cells were maintained in the undifferentiated
496 state by cultivation in poor DMEM medium (Gibco, Ref. 21068-028) supplemented with 1X
497 glutaMax (Gibco, Ref. 35050-038), 1X sodium pyruvate (Gibco, Ref. 11360-039), 2 % fetal
498 bovine serum and 8 % chelated fetal bovine serum using Chelex® 100 Resin (BioRad, Ref. 142-
499 1253). To differentiate HaCaT cells, 2.8 mM $CaCl_2$ (Sigma-Aldrich, Ref. 21115) was added to
500 the medium. Cells were differentiated after seven days as described [46]. All cell lines were
501 routinely evaluated for cellular morphology and growth characteristics by microscopy.
502
503 **Bacterial adhesion capacity**
504 GAS adhesion capacity was evaluated as described after growing bacteria in THY to an OD_{600}
505 of 0.4 to 0.5 [34]. Values were normalized to the inoculum for each experiment.
506
507 **Bacterial growth capacity in the presence of eukaryotic cells or culture supernatants**
508 GAS were cultured in THY to OD_{600} = 0.4 - 0.5. Bacteria were washed twice in PBS and diluted
509 in RPMI medium without glutamine (Gibco, Ref. 32404-014) to infect cell cultures or inoculate
510 filtered cell culture supernatants (conditioned supernatants) at a final concentration of 10^3 and
511 10^4 bacteria per ml, respectively. Confluent cells in 24-well plates were starved 24 h before the
512 experiment, *i.e.* incubated in RPMI medium without glutamine, and washed twice in PBS. Cells
513 were infected with 1 ml of bacteria and incubated at 37 °C + 5 % CO_2. After 8 h, supernatants
514 were recovered and cells were lysed with 1 ml distilled water. The fractions were pooled and
515 serial dilutions plated on THYA plates. Conditioned supernatants were prepared by incubating
516 cells in 1 ml RPMI at 37 °C + 5 % CO_2 for 8 h. The conditioned supernatant was recovered,
517 inoculated with 10^3 bacteria, and incubated for another 4, 8, 16 or 24 h. Serial dilutions were

518 plated on THYA plates. The number of cfus was determined after 24 h of growth at 37 °C and
519 normalized to the inoculum for each experiment.
520
521 **Live / dead analysis**
522 After bacterial growth in the HEC-1-A conditioned supernatant during 8 h, bacterial mortality
523 was determined using the LIVE/DEAD® BacLightTM Bacterial Viability Kit (ThermoFisher
524 Scientific, Ref. L7012) as described for flow cytometry utilization using an ACCURI C6
525 cytometer (BD Biosciences, Le pont de Claix,France) from the CYBIO Core Facility. Bacteria
526 were grown in HEC-1-A conditioned supernatant for 8 h for testing. Results of three
527 independent experiments were analyzed using the BD Accuri C6 software.
528
529 **Metabolomic analysis**
530 HEC-1-A conditioned supernatants were inoculated or not with WT or mFabT strains during 8
531 or 16 h and prepared as described above (see 'Bacterial growth capacity in the presence of
532 eukaryotic cells or culture supernatants'). The metabolite composition of these supernatants
533 was analyzed by Proteigene (https://proteigene.com) using MxP® Quant 500 kit (Biocrates) by
534 two analytical methods, LC-MS/MS for small molecules and FIA-MS/MS for lipids. This
535 analysis was repeated on 3 independent series of supernatants and on RPMI. These analyses
536 have a defined detection threshold (LOD) for each family of metabolite. Metabolomic data were
537 deposited in the Mendeley database: https://data.mendeley.com/datasets/5cnyvy7vvf/2.
538
539 **Spontaneous *fabT* mutant isolation**
540 WT strain overnight precultures were diluted in THY and grown at 37 °C. When the THY
541 culture reached mid-exponential phase, (OD_{600} = 0.4 - 0.5), bacteria were either diluted 1/10
542 and transferred to THY-C14:0 supplemented with BSA 0.025 %, or $1.5x10^7$ cfu were streaked

543 on THYA supplemented with C14:0 (THYA-C14:0). The THY-C14:0 liquid culture and plates
544 were incubated 60 h at 37 °C. THY-C14:0 liquid cultures were subsequently streaked on
545 THYA-C14:0 plates. Thirteen and six colonies were isolated, respectively from the THY-C14:0
546 liquid then THYA-C14:0 plates, and THYA-C14:0 plates. Isolated colonies were subsequently
547 grown on THYA. Eight colonies issued from the liquid selection, and all six clones from the
548 solid medium were used for *fabT* sequencing; PCR was performed directly on patched colonies.
549 The oligonucleotides used were FabT-222, and FabTavComp, (Supplementary Table 8) binding
550 221 bp 5' from the T of the TTG translation start site and 565 bp downstream of it, respectively.
551 The *fabT* gene and surrounding sequences were amplified by PCR using the Green Taq DNA
552 Polymerase, GenScript, according to the manufacturer's instruction, with 30 cycles with a
553 hybridizing temperature of 50 °C and an elongation time of 1 min. Sanger sequencing was
554 carried out by Eurofin Genomics (https://eurofinsgenomics.eu/en/custom-dna-
555 sequencing/portfolio-overview/) on PCR products. These analyses identifed $FabT^{T65M}$ in all
556 eight sequenced clones from liquid selection, and $FabT^{G99S}$ in one of six clones on solid
557 medium; the other clones displayed a WT FabT.
558

559 ***Ex vivo* assessment of GAS WT and mFabT growth on muscle (meat) lipids**

560 $WT^{eryR\text{-}igfp}$ and $mFabT^{eryR\text{-}igfp}$ strains (Supplementary Table 7) [23] were grown overnight in BHI
561 (Ery 5), and then diluted to OD_{600} = 0.05 in FA-free bovine serum albumin (referred to as BSA;
562 0.025%) plus C17:1 100 µM in 1 ml, without or with platensimycin 1 µg/ml, with Ery 5 for
563 selection. After 4 h growth, culture densities were adjusted to OD_{600} = 1 in BHI, and 35 µl were
564 spread on 5 cm diameter plates containing 5 ml BHI agar plus BSA 0.025 % and C17:1 100
565 µM, without or with platensimycin 0.5 µg/ml, with Ery 5 for selection. The muscle samples
566 used were from organic cattle meat bought frozen and pre-ground, containing 15 % fat (as
567 declared by supplier; Picard, France). Absence of contaminants was checked by plating without

568 bacteria. Samples were placed directly on the lawns, and plates were incubated 48 h at 37 °C,
569 and photographed. N=4 for experiments without platensimycin, and N=2 for those with
570 platensimycin.
571
572 **Statistical analysis**
573 Data were analyzed with GraphPad Prism version 9.4.1. The tests used are indicated in figure
574 legends. Statistical significance is indicated by: ns (not significant, $p > 0.05$); *, $p < 0.05$; **,
575 $p < 0.01$; ***, $p < 0.001$; ****, $p < 0.0001$. In addition, the Shapiro-Wilk normality test was
576 used for all t-tests.
577
578 **Data availability.** All relevant data are within the manuscript, supporting information files,
579 and depositories. Transcriptome, metabolome data were deposited in the Mendeley repository
580 (respectively https://data.mendeley.com/datasets/68bhhsy2p4/1 and
581 https://data.mendeley.com/datasets/5cnyvy7vvf/2). Lipidomics were deposited in the
582 Mendeley database in MZML open-source format
583 (https://data.mendeley.com/datasets/cf578v8d8b/1). All data are publicly available as of
584 publication. Any additional information required to reanalyze the data reported in this paper
585 is available from the authors upon request.
586
587
588 **References**
589
590 1 Jerga, A. & Rock, C. O. Acyl-Acyl carrier protein regulates transcription of fatty acid
591 biosynthetic genes via the FabT repressor in *Streptococcus pneumoniae*. *J Biol Chem*
592 **284**, 15364-15368, doi:10.1074/jbc.C109.002410 (2009).
593 2 Lambert, C. *et al.* Acyl-AcpB, a FabT corepressor in Streptococcus pyogenes. *J*
594 *Bacteriol* **205**, e0027423, doi:10.1128/jb.00274-23 (2023).
595 3 Lambert, C., Poyart, C., Gruss, A. & Fouet, A. FabT, a Bacterial Transcriptional
596 Repressor That Limits Futile Fatty Acid Biosynthesis. *Microbiol Mol Biol Rev*,
597 e0002922, doi:10.1128/mmbr.00029-22 (2022).

598 4 Zou, Q., Zhu, L. & Cronan, J. E. The *Enterococcus faecalis* FabT transcription factor
599 regulates fatty acid synthesis in response to exogenous fatty acids. *Front Microbiol* **13**,
600 877582, doi:doi: 10.3389/fmicb.2022.877582 (2022).
601 5 Eraso, J. M. *et al.* Genomic Landscape of Intrahost Variation in Group A *Streptococcus*:
602 Repeated and Abundant Mutational Inactivation of the *fabT* Gene Encoding a Regulator
603 of Fatty Acid Synthesis. *Infect Immun* **84**, 3268-3281, doi:10.1128/IAI.00608-16
604 (2016).
605 6 Lu, Y. J. & Rock, C. O. Transcriptional regulation of fatty acid biosynthesis in
606 *Streptococcus pneumoniae*. *Mol Microbiol* **59**, 551-566, doi:10.1111/j.1365-
607 2958.2005.04951.x (2006).
608 7 Eckhardt, T. H., Skotnicka, D., Kok, J. & Kuipers, O. P. Transcriptional regulation of
609 fatty acid biosynthesis in *Lactococcus lactis*. *J Bacteriol* **195**, 1081-1089,
610 doi:10.1128/JB.02043-12 (2013).
611 8 Faustoferri, R. C. *et al.* Regulation of fatty acid biosynthesis by the global regulator
612 CcpA and the local regulator FabT in *Streptococcus mutans*. *Mol Oral Microbiol* **30**,
613 128-146, doi:10.1111/omi.12076 (2015).
614 9 Zhang, J. *et al.* Inactivation of Transcriptional Regulator FabT Influences Colony Phase
615 Variation of *Streptococcus pneumoniae*. *mBio* **12**, e0130421, doi:10.1128/mBio.01304-
616 21 (2021).
617 10 Barnett, T., Indraratna, A. & Sanderson-Smith, M. in *Streptococcus pyogenes: Basic*
618 *Biology to Clinical Manifestations* (eds J. J. Ferretti, D. L. Stevens, & V. A. Fischetti)
619 Ch. 13, (2022).
620 11 Carapetis, J. R., Steer, A. C., Mulholland, E. K. & Weber, M. The global burden of
621 group A streptococcal diseases. *Lancet Infect Dis* **5**, 685-694, doi:S1473-
622 3099(05)70267-X [pii] 10.1016/S1473-3099(05)70267-X (2005).
623 12 Tatsuno, I. *et al.* Relevance of spontaneous *fabT* mutations to a streptococcal toxic
624 shock syndrome to non-streptococcal toxic shock syndrome transition in the novel-type
625 *Streptococcus pyogenes* isolates that lost a salRK. *APMIS* **124**, 414-424,
626 doi:10.1111/apm.12521 (2016).
627 13 Longo, M. *et al.* Complete Genome Sequence of *Streptococcus pyogenes emm28*
628 Clinical Isolate M28PF1, Responsible for a Puerperal Fever. *Genome Announc* **3**,
629 doi:10.1128/genomeA.00750-15 (2015).
630 14 Lambert, C. *et al.* A *Streptococcus pyogenes* DegV protein regulates the membrane lipid
631 content and limits the formation of extracellular vesicles. *PLoS One* **18**, e0284402,
632 doi:10.1371/journal.pone.0284402 (2023).
633 15 Zuo, G. *et al.* Structural insights into repression of the Pneumococcal fatty acid
634 synthesis pathway by repressor FabT and co-repressor acyl-ACP. *FEBS Lett* **593**, 2730-
635 2741, doi:10.1002/1873-3468.13534 (2019).
636 16 Haines, T. H. & Dencher, N. A. Cardiolipin: a proton trap for oxidative phosphorylation.
637 *FEBS Lett* **528**, 35-39, doi:10.1016/s0014-5793(02)03292-1 (2002).
638 17 Port, G. C., Vega, L. A., Nylander, A. B. & Caparon, M. G. *Streptococcus pyogenes*
639 polymyxin B-resistant mutants display enhanced ExPortal integrity. *J Bacteriol* **196**,
640 2563-2577, doi:10.1128/JB.01596-14 (2014).
641 18 Teuber, M. & Miller, I. R. Selective binding of polymyxin B to negatively charged lipid
642 monolayers. *Biochim Biophys Acta* **467**, 280-289, doi:10.1016/0005-2736(77)90305-4
643 (1977).
644 19 Rosinski-Chupin, I., Sauvage, E., Fouet, A., Poyart, C. & Glaser, P. Conserved and
645 specific features of *Streptococcus pyogenes* and *Streptococcus agalactiae*
646 transcriptional landscapes. *BMC Genomics* **20**, 236, doi:10.1186/s12864-019-5613-5
647 (2019).

20 Zhu, L. *et al.* Contribution of Secreted NADase and Streptolysin O to the Pathogenesis of Epidemic Serotype M1 *Streptococcus pyogenes* Infections. *Am J Pathol* **187**, 605-613, doi:10.1016/j.ajpath.2016.11.003 (2017).
21 Green, N. M. *et al.* Genome sequence of a serotype M28 strain of group a streptococcus: potential new insights into puerperal sepsis and bacterial disease specificity. *J Infect Dis* **192**, 760-770, doi:JID33878 [pii] 10.1086/430618 (2005).
22 Plainvert, C. *et al.* Invasive group A streptococcal infections in adults, France (2006-2010). *Clin Microbiol Infect* **18**, 702-710, doi:10.1111/j.1469-0691.2011.03624.x (2012).
23 Weckel, A. *et al. Streptococcus pyogenes* infects human endometrium by limiting the innate immune response. *J Clin Invest* **131**, doi:10.1172/JCI130746 (2021).
24 Pancholi, V. & Caparon, M. in *Streptococcus pyogenes : Basic Biology to Clinical Manifestations* (eds J. J. Ferretti, D. L. Stevens, & V. A. Fischetti) (2016).
25 Vadia, S. *et al.* Fatty Acid Availability Sets Cell Envelope Capacity and Dictates Microbial Cell Size. *Curr Biol* **27**, 1757-1767 e1755, doi:10.1016/j.cub.2017.05.076 (2017).
26 Wang, J. *et al.* Platensimycin is a selective FabF inhibitor with potent antibiotic properties. *Nature* **441**, 358-361, doi:10.1038/nature04784 (2006).
27 Thormar, H. & Hilmarsson, H. The role of microbicidal lipids in host defense against pathogens and their potential as therapeutic agents. *Chem Phys Lipids* **150**, 1-11, doi:10.1016/j.chemphyslip.2007.06.220 (2007).
28 Ni Raghallaigh, S., Bender, K., Lacey, N., Brennan, L. & Powell, F. C. The fatty acid profile of the skin surface lipid layer in papulopustular rosacea. *Br J Dermatol* **166**, 279-287, doi:10.1111/j.1365-2133.2011.10662.x (2012).
29 Tsujii, H., Matsuoka, Y., Obata, R., Hossain, M. S. & Takagi, Y. Fatty acid composition of lipids in day 7-13 blastocysts, serum and uterine fluid of rabbits. *Reprod Med Biol* **8**, 107-112, doi:10.1007/s12522-009-0020-2 (2009).
30 Young, H. J., Jenkins, N. T., Zhao, Q. & McCully, K. K. Measurement of intramuscular fat by muscle echo intensity. *Muscle Nerve* **52**, 963-971, doi:10.1002/mus.24656 (2015).
31 Brinster, S. *et al.* Type II fatty acid synthesis is not a suitable antibiotic target for Gram-positive pathogens. *Nature* **458**, 83-86, doi:10.1038/nature07772 (2009).
32 Kenanian, G. *et al.* Permissive Fatty Acid Incorporation Promotes Staphylococcal Adaptation to FASII Antibiotics in Host Environments. *Cell Rep* **29**, 3974-3982 e3974, doi:10.1016/j.celrep.2019.11.071 (2019).
33 Hays, C. *et al.* Type II Fatty Acid Synthesis Pathway and Cyclopropane Ring Formation Are Dispensable during Enterococcus faecalis Systemic Infection. *J Bacteriol* **203**, e0022121, doi:10.1128/JB.00221-21 (2021).
34 Weckel, A. *et al.* The N-terminal domain of the R28 protein promotes *emm28* group A *Streptococcus* adhesion to host cells via direct binding to three integrins. *J Biol Chem* **293**, 16006-16018, doi:10.1074/jbc.RA118.004134 (2018).
35 Six, A. *et al.* Srr2, a multifaceted adhesin expressed by ST-17 hypervirulent Group B *Streptococcus* involved in binding to both fibrinogen and plasminogen. *Mol Microbiol* **97**, 1209-1222, doi:10.1111/mmi.13097 (2015).
36 Abreu, S., Solgadi, A. & Chaminade, P. Optimization of normal phase chromatographic conditions for lipid analysis and comparison of associated detection techniques. *J Chromatogr A* **1514**, 54-71, doi:10.1016/j.chroma.2017.07.063 (2017).
37 Bligh, E. G. & Dyer, W. J. A rapid method of total lipid extraction and purification. *Can J Biochem Physiol* **37**, 911-917, doi:10.1139/o59-099 (1959).

38 Thedieck, K. *et al.* The MprF protein is required for lysinylation of phospholipids in listerial membranes and confers resistance to cationic antimicrobial peptides (CAMPs) on Listeria monocytogenes. *Mol Microbiol* **62**, 1325-1339, doi:10.1111/j.1365-2958.2006.05452.x (2006).
39 Moulin, M. *et al.* Sex-specific cardiac cardiolipin remodelling after doxorubicin treatment. *Biol Sex Differ* **6**, 20, doi:10.1186/s13293-015-0039-5 (2015).
40 Anders, S. *et al.* Count-based differential expression analysis of RNA sequencing data using R and Bioconductor. *Nat Protoc* **8**, 1765-1786, doi:10.1038/nprot.2013.099 nprot.2013.099 [pii] (2013).
41 Varet, H., Brillet-Gueguen, L., Coppee, J. Y. & Dillies, M. A. SARTools: A DESeq2- and EdgeR-Based R Pipeline for Comprehensive Differential Analysis of RNA-Seq Data. *PLoS One* **11**, e0157022, doi:10.1371/journal.pone.0157022 (2016).
42 Benjamini, Y. & Hochberg, Y. Controlling the False Discovery Rate: A Practical and Powerful Approach to Multiple Testing. *J Royal Statistical Society Series B* **57**, 289-300, doi:10.1111/j.2517-6161.1995.tb02031.x (1995).
43 Lex, A., Gehlenborg, N., Strobelt, H., Vuillemot, R. & Pfister, H. UpSet: Visualization of Intersecting Sets. *IEEE Trans Vis Comput Graph* **20**, 1983-1992, doi:10.1109/TVCG.2014.2346248 (2014).
44 Conway, J. R., Lex, A. & Gehlenborg, N. UpSetR: an R package for the visualization of intersecting sets and their properties. *Bioinformatics* **33**, 2938-2940, doi:10.1093/bioinformatics/btx364 (2017).
45 Marcellin, L. *et al.* Immune Modifications in Fetal Membranes Overlying the Cervix Precede Parturition in Humans. *J Immunol* **198**, 1345-1356, doi:10.4049/jimmunol.1601482 (2017).
46 Malerba, M. *et al.* Epidermal hepcidin is required for neutrophil response to bacterial infection. *J Clin Invest* **130**, 329-334, doi:10.1172/JCI126645 (2020).

Acknowledgments and Funding

Expert assistance of Benjamin Saint-Pierre (Genom'IC facility of the Institut Cochin) with transcriptomic experiments is gratefully acknowledged. We thank Alice d'Orfani, Lauryn Moali, Iman Nasr and Laure Detheve, undergraduates in the laboratory for technical help, the Imag'IC and Cybio core facilities of the Institut Cochin, and Cédric Broussard, Virginie Salnot and François Guillonneau for helpful discussions. We are grateful to Jamila Anba-Mondoloni (Micalis Institute) for provided valuable comments and suggestions on this work. We thank the personnel of the CIC Mère-Enfant Cochin-Necker for the human decidua, and the MELISA core facility for supporting this work. We acknowledge the use of Alphafold and ChimeraX for FabT *in silico* design, and BioRender for computer-generated models.

CL was supported by Université Paris Cité (BioSPC, n° 51809666), FRM (FDT202106012831) and FEMS (FEMS Congress Attendance Grant for poster n° 7875 in 2021 and FEMS grant - LISSSD 2022 n° LISS-213065). This work was supported by DIM One Health (RPH17043DJA) (AF), Agence Nationale de la Recherche (ANR-16-CE15-0013 and JPIAMR ANR-22-AAMR-0007 projects; AG), and the Fondation pour la Recherche Medicale (DBF20161136769) (AG). IMAG'IC core facility is supported by the National Infrastructure France BioImaging (grant ANR-10-INBS-04).

Author Contributions

CL, MG, PW, CB, AH, KG, CM, BP, AS, SA, MA, AG, and AF performed and interpreted experiments. CL, PW, TG, BP, AS, CP, AG, and AF analyzed and interpreted data. CL, AG, and AF conceived the project, designed research, and wrote the paper.

Competing interests

The authors declare no competing interests.

750 **Figure legends**
751
752 **Fig. 1 | FA differences in WT and mFabT strains impact lipid content and composition.**
753 **a, b,** HPLC-MS profiles represent the main lipid classes in WT and mFabT grown in indicated
754 media to OD_{600}=0.5; lipid profiles and quantifications by class. Lipid concentrations correspond
755 to milligrams extracted from OD_{600}=100 equivalents. MGDG, monoglucosyldiacylglycerol;
756 DGDG, diglucosyldiacylglycerol ; PG, phosphatidylglycerol; CL, cardiolipin (Supplementary
757 Table 3). **c, d, e** CL species in WT and mFabT, showing deoxidized cardiolipin (deoxy-CL)
758 species (indicated by a 'd' preceding the identification name; see Supplementary Table 2); **a-b,**
759 N=4; **c-d,** N=3. **a, b, e,** 2-way ANOVA, Bonferroni post-test, **p<0.01; ***p<0.001. **f,**
760 Polymyxin B sensitivity. WT and mFabT were precultured to OD_{600} = 0.5 in THY or THY-
761 Tween and dilutions were spotted on the same respective solid medium supplemented or not
762 with polymyxin B (PB). Plates are representative of 3 independent experiments. **a-d**, NL,
763 normalization level; WT, white bars; mFabT, green bars.
764
765 **Fig. 2 | FabT regulon in the presence of eFAs and genetic organization of the GAS FASII**
766 **genes. a,** Schematic representation of the GAS FabT regulon, comprising genes of the FASII
767 locus and *fakB4*. Gene positions with names below are represented. Red asterisks, putative
768 FabT binding sites [3]; bent arrows, transcription start sites; solid arrow, transcript defined by
769 RT-PCRs; dotted arrows, transcripts from previously reported start sites [19]. **b-e**, Volcano plots
770 of differentially expressed genes, compared as indicated. See supplementary Table 4 for a
771 complete list. Volcano plots were constructed using GraphPad Prism, by plotting the negative
772 base 10 logarithm of the p-value on the y axis, and the log of the fold change (base 2) on the x
773 axis. P-values for comparisons of peak intensities were calculated by t-tests. Padj: calculated p-
774 values were adjusted for multiple testing using the false discovery rate controlling procedure
775 (see Methods section). Gene expression was considered modified in a given condition when the
776 absolute value of log2-Foldchange (FC) was greater than or equal to 1, with an adjusted p-value
777 ≤ 0.05. Data points with low p-values (highly significant) appear at the top of the plot.
778
779 **Fig. 3 | The mFabT strain grows poorly on human tissue *ex vivo* and displays adhesion**
780 **and growth defects in the presence of human cells or in conditioned cell supernatant. a,**
781 Comparison of GAS WT and mFabT cfus after 8 h growth in static conditions in the presence
782 of human decidua tissue. **b-c,** Bacterial multiplication at the tissue surface in flow conditions
783 (live imaging); **b, left,** Visualization of $WT^{eryR\text{-}igfp}$ and $mFabT^{eryR\text{-}igfp}$ multiplication in 2D. As
784 poor mFabT growth led to nearly identical images at 1 and 4 h, differences are highlighted by
785 arrowheads; **right,** ratios of areas covered by the two strains. **c, left**, 3D-surface heatmap of
786 bacterial layer thickness at 1 and 4 h. The x, y, and z axes are scaled, color code in µm; **right,**
787 quantification of bacterial layer mean thickness of $WT^{eryR\text{-}igfp}$ and $mFabT^{eryR\text{-}igfp}$ strains on
788 decidual tissue. **d-g**, Comparison of WT and mFabT strain adhesion and growth capacities in
789 the presence of human cells, or conditioned supernatants. Endometrial cells, undifferentiated
790 keratinocytes, and differentiated keratinocytes, and their respective conditioned supernatants
791 were used as specified. **d**, adhesion; **e-f,** growth ($cfu.mL^{-1}$). **g, left,** Bacterial growth kinetics in
792 endometrial conditioned supernatants; **right,** Live/Dead bacteria assessment after 8 h growth
793 in conditioned supernatants. Growth experiments were started with 10^3 bacteria per ml.

794 Determinations were based on N=5 for **a**, N=3 for **b**, **c**, **g,** N=9, 7, 7 for **d** (left to right), N=11,
795 9, 6 for **e** (left to right) and N=8, 7, 9 for **f** (left to right). Analyses were done by T test and
796 Wilcoxon test for **a**, **d-f** and 2-way ANOVA, Bonferroni post-test for **b**, **c**, **g**; *p<0.05;
797 **p<0.01; ***p<0.001; ****p<0.0001. **d-f**, Outliers were searched using ROUT method
798 (GraphPad), with Q=1 %. **d-g:** WT, white bars; mFabT, green bars.
799
800 **Fig. 4 | The mFabT strain is more energy-consuming than the WT strain.** Metabolomic
801 analysis of conditioned supernatants inoculated with WT or mFabT after 8 or 16 h incubation.
802 Carbohydrate and amino acid consumption by the two strains are compared (see Supplementary
803 Fig. 5 for metabolite levels in noninfected samples, and Supplementary Table 5 for further
804 amino acid results). N=3, 2-way ANOVA, Bonferroni post-test; *p<0.05; **p<0.01;
805 ***p<0.005; p-values just above the p=0.05 threshold are indicated. Strains and growth times
806 are below.
807
808 **Fig. 5 | The eFA incorporation defect of mFabT confers a selective advantage in saturated**
809 **eFA environments, and in a simulated muscle biotope. a,** FA membrane composition of WT
810 and mFabT strains grown in THY-C17:1 (100 µM), containing or not the FASII-inhibitor
811 platensimycin (1 µg/mL^{-1}). **Left**, FA profiles; **right**, quantified proportions of major FAs. Both
812 strains grew in C17:1 regardless of the presence of platensimycin (Supplementary Table 6). **b,**
813 Growth of WT (left), and mFabT (right) in THY supplemented with 100 µM saturated FAs,
814 C14:0 or C16:0 and BSA 0.025%. **c, Left,** Incorporation of exogenous C14:0 and C16:0 from
815 cultures described in '**b**'. **Right**, Percent C14:0 and C16:0 incorporation from growth
816 experiments at left. For these analyses, N=3, 2-way ANOVA, Bonferroni post-test, *p<0.05;
817 **p<0.01; ***p<0.001. WT (black lines, white bars) and mFabT (green lines and bars). **d-e,**
818 The indicated strains were spread on solid BHI medium. Pellets of organic ground bovine meat
819 (~15 % fat), used as muscle source, were placed on the bacterial lawns. Plates were
820 photographed 36 h after incubation at 37 °C. Arrowheads indicate zones of inhibition (white)
821 or growth (black) around muscle sources. N=4. **d, Upper**,WT$^{eryR\text{-}igfp}$ and mFabT$^{\text{eryR-}igfp}$ strains
822 were grown in BHI Ery 5, and plated on the same solid medium. **Lower**, schematic
823 representation of GAS strain growth inhibition and stimulation by muscle. **e,** mFabT$^{eryR\text{-}igfp}$ was
824 grown in BHI Ery 5 medium containing C17:1 as FA source, without or with platensimycin to
825 turn off FASII. Cultures were then plated on respectively the same solid medium. N=2.
826
827 **Fig. 6 | Model for emergence of *fabT* mutants that are attenuated for virulence. a,**
828 **Saturated FAs (SFAs) in a lipid environment favor mFabT emergence**. Toxic FAs may be
829 present in initial GAS contacts with the host. Counter-selection would lead to emergence of
830 FA-insensitive *fabT* mutants, conferring a growth advantage. In a proof of concept, we show
831 that *fabT* mutants are selected in an SFA environment. **b, Host cell environment during**
832 **invasion hinders mFabT growth**. Compared to the WT, *fabT* mutant bacteria fail to develop
833 and die more rapidly when exposed to human cells; they are also impaired for adhesion. Longer
834 SFAs and continued FASII activity in *fabT* mutants provokes a state of futile bacterial
835 metabolism where metabolite uptake is stimulated, but does not lead to improved growth. Thus,
836 *fabT* mutants in GAS populations may confer a survival advantage at the inoculation site, but

do not withstand host cell infection conditions. Mauve and green circles, WT and mFabT cocci; zoom is on phospholipids. Small yellow circles and lines, lipids and eFA hydrolysis products respectively, small red, blue, pink circles, sugars and amino acid residues. Figure was drawn using BioRender (BioRender.com).

Supplementary Figures

Supplementary Fig. 1 | FabT regulator and FASII pathway in GAS. a, The FASII synthesis pathway comprises a first initiation phase for precursor synthesis, followed by the recursive elongation cycle. The final product, acyl-ACP, supplies FAs for phospholipid synthesis. FabM (orange) leads to unsaturated *cis* FAs; FabK products are saturated. Initiation phase and elongation cycle enzymes are represented in green and red, respectively. From [1]. **b,** FabT sequence; amino acids involved in DNA binding are in red, and those interacting with acyl-Acyl carrier protein are in blue. Arrow indicates the His105Tyr FabT mutation studied in this work. Magenta stars highlight amino acids spontaneously mutated *in vivo* and in a saturated-FA environment (this work). **c,** Overall structure of FabT dimer predicted by Alphafold and adapted with ChimeraX (see references 1-2 in supplementary Methods); one monomer is represented as multicolored (each color designates a separate domain), and the other is beige. Residues Thr65, Gly99 and His105, in magenta, correspond to mutants isolated in this study.

1. Lambert, C., Poyart, C., Gruss, A. & Fouet, A. FabT, a Bacterial Transcriptional Repressor That Limits Futile Fatty Acid Biosynthesis. *Microbiol Mol Biol Rev*, e0002922, doi:10.1128/mmbr.00029-22 (2022).

Supplementary Fig. 2 | Impact of FabT mutations on GAS growth. a-d, WT growth was compared to mFabT (**a** and **b** left; adapted from reference 1) or to Δ*fabT* (**c** and **d**) on THY and THY-Tween. Viability tests (**a** and **b,** right), using the LIVE/DEAD® BacLightTM Bacterial Viability Kit, were performed on WT and mFabT cultures after growth to OD_{600} = 0.4 - 0.5. Legend at the right of **d** is for growth curves. **e,** Ratios of CFUs of WT or mFabT strains after 8 h over respective initial inocula (10^3/ml for each) in RPMI medium; ratio below 1 indicates that bacteria die. **f**, Real-time growth of WT and mFabT in endometrial conditioned supernatant followed using Live-Cell Analysis System (IncuCyte®, Sartorius) and the Basic analyzer. **a-d**, **e**, N=3; **f** N=10; differences in **a, b,** and **e** were not statistically significant using T-test. **a, b, e**, Outliers were searched using ROUT method (GraphPad), with Q=1 %. WT, black lines or white bars; mFabT, green lines or bars.

1. Lambert, C. *et al.* Acyl-AcpB, a FabT corepressor in Streptococcus pyogenes. *J Bacteriol* **205**, e0027423, doi:10.1128/jb.00274-23 (2023).

Supplementary Fig. 3 | Phospholipid membrane composition. Identification of **a**, monoglucosyldiacylglycerol (MGDG), **b**, diglucosyldiacylglycerol (DGDG), **c**, phosphatidylglycerol (PG), **d**, cardiolipin (CL) and deoxidized cardiolipin (Deoxy-CL). For each class, lipids are presented as the percentage of total lipids, and are quantified in

881 Supplementary Table 2. For **a**, **b**, and **c**, fatty acid assignments are presented directly on mass
882 spectrometry analyses. Cardiolipin assignments were ambiguous and are not shown. Statistical
883 values were determined using 2-way ANOVA, Bonferroni post-test. *p<0.05; **p<0.01;
884 ***p<0.001; ****p<0.0001. Strains were grown in THY (open bars) and THY-Tween (hatched
885 bars). WT, black lines and white bars; mFabT, green lines and bars.
886
887 **Supplementary Fig. 4 | Impact of mFabT on FASII and non-FASII gene expression in the**
888 **absence of FA supplementation**. **a-c**, WT and mFabT strains were grown in THY medium. **a,**
889 **c**, RNAs were quantified by qRT-PCR. Expression was normalized to that of *gyrA;* relative
890 gene expression is expressed as the log2-fold ratio. **a,** FASII gene expression of mFabT relative
891 to WT is reproduced from Reference 1**. b**, mRNA transcript analysis of FASII locus genes:
892 agarose gel of PCR amplification products on cDNA using primer pairs from neighboring
893 genes. MW, molecular weight reference (Generuler 100 bp, ThermoFisher Scientific). Lane 1,
894 *fabM-fabT* (234 bp); 2, *fabH-acpA* (221 bp); 3, *acpA-fabK* (302 bp); 4, *fabZ-accC* (105 bp); 5,
895 *accD-serS* (288 bp). Results confirm the FASII transcriptional units indicated in Fig. 2a. **c**,
896 expression of non-FASII genes in WT and mFabT strains **(**see Supplementary Table 1 for gene
897 assignments**)**. The relative gene expression is expressed as the log2-fold ratio in a given strain
898 grown in THY-Tween vs in THY. *, significance of differences in the two media between WT
899 and mFabT. In **a-c,** WT, white bars; mFabT, green bars. **a, b**, N=4; **c**, N=3. **a-c**, 2-way ANOVA,
900 Bonferroni post-test *p<0.05; ****p<0.0001. **c**, expression of non-FASII genes in WT and
901 mFabT strains **(**see Supplementary Table 1 for gene assignments**).** In **a-c,** WT, white bars;
902 mFabT, green bars. **a, b**, N=4; **c**, N=3. **a-c**, 2-way ANOVA, Bonferroni post-test *p<0.05;
903 ****p<0.0001.
904
905 1. Lambert, C. *et al.* Acyl-AcpB, a FabT corepressor in Streptococcus pyogenes. *J Bacteriol*
906 **205**, e0027423, doi:10.1128/jb.00274-23 (2023).
907
908 **Supplementary Fig. 5 | Carbohydrates and amino acid residues produced by human**
909 **endometrial cells.** Metabolomic analysis of RPMI and HEC-1-A conditioned supernatants, as
910 per legend at right. (see Supplementary Table 5 for complete data). N=3, 2-way ANOVA,
911 Bonferroni post-test; *p<0.05; ***p<0.005; ****p<0.001.
912
913 **Supplementary Fig. 6. FabT mutant growth and FA profiles in the absence and presence**
914 **of exogenous C14:0.** Triplicate cultures of the two isolated *fabT* mutants ($FabT^{T65M}$ and
915 $FabT^{G99S}$) and controls (WT, mFabT, Δ*fabT*) were prepared in BHI medium with 0.025 % BSA.
916 Medium was without (left column), or with 100 µM C14:0 (right column). OD_{600} is shown for
917 each strain and both conditions after 4 h growth (boxed). For each strain, proportions of C14:0
918 present in FA profiles of WT and *fabT* mutant strains are in red; proportions, from left to right,
919 of C16:0, C18:0, C18:1Δ9 and C18:1Δ11 are in black.
920

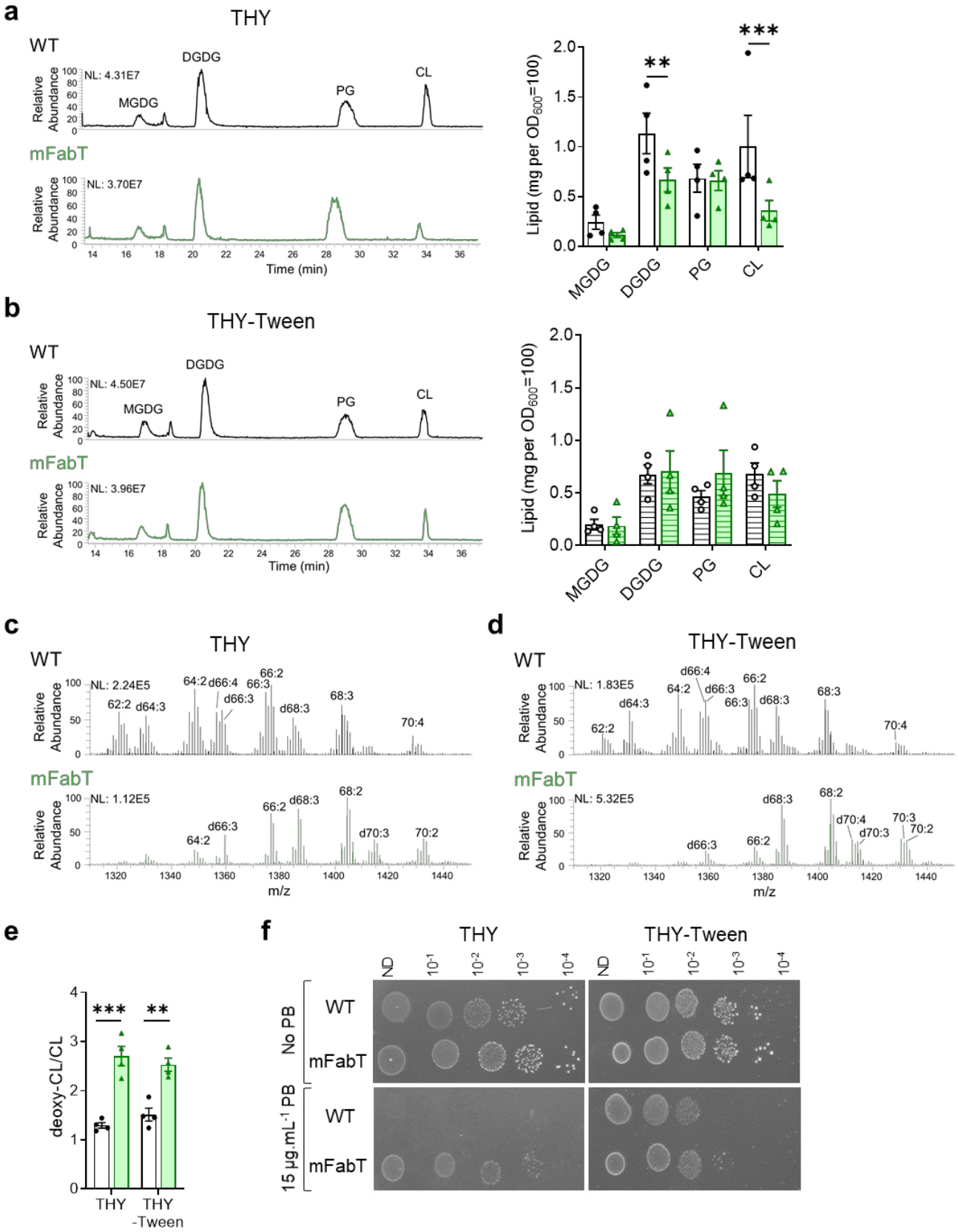
a
THY
WT
NL: 4.31E7
MGDG
DGDG
PG
CL
mFabT
NL: 3.70E7
Relative Abundance
Time (min)
Lipid (mg per OD600=100)
MGDG
DGDG
PG
CL
b
THY-Tween
WT
NL: 4.50E7
mFabT
NL: 3.96E7
c
THY
WT
NL: 2.24E5
mFabT
NL: 1.12E5
m/z
d
THY-Tween
WT
NL: 1.83E5
mFabT
NL: 5.32E5
e
deoxy-CL/CL
THY
THY -Tween
f
THY
THY-Tween
ND
No PB
15 µg.mL-1 PB
WT
mFabT

Fig. 1

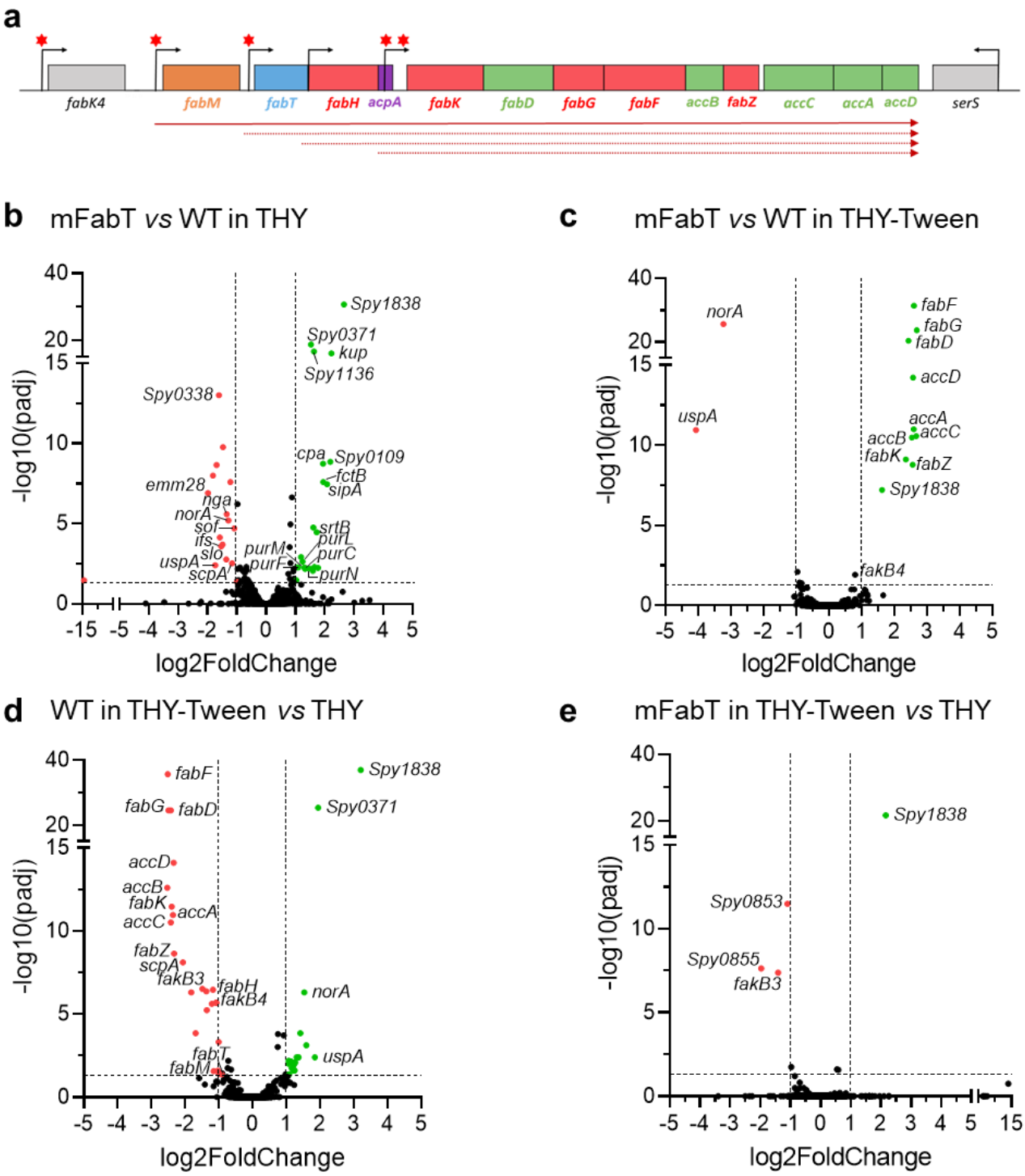
a
fabK4
fabM
fabT
fabH
acpA
fabK
fabD
fabG
fabF
accB
fabZ
accC
accA
accD
serS
b mFabT vs WT in THY
-log10(padj)
log2FoldChange
Spy1838
Spy0371
kup
Spy1136
Spy0338
cpa
Spy0109
fctB
sipA
emm28
nga
norA
sof
srtB
ifs
purL
slo
purM
purC
uspA
purF
scpA
purN
c mFabT vs WT in THY-Tween
-log10(padj)
log2FoldChange
norA
fabF
fabG
fabD
accD
uspA
accA
accC
accB
fabK
fabZ
Spy1838
fakB4
d WT in THY-Tween vs THY
-log10(padj)
log2FoldChange
fabF
Spy1838
fabG
fabD
Spy0371
accD
accB
fabK
accA
accC
fabZ
scpA
fakB3
fabH
fakB4
norA
fabT
fabM
uspA
e mFabT in THY-Tween vs THY
-log10(padj)
log2FoldChange
Spy1838
Spy0853
Spy0855
fakB3

Fig. 2

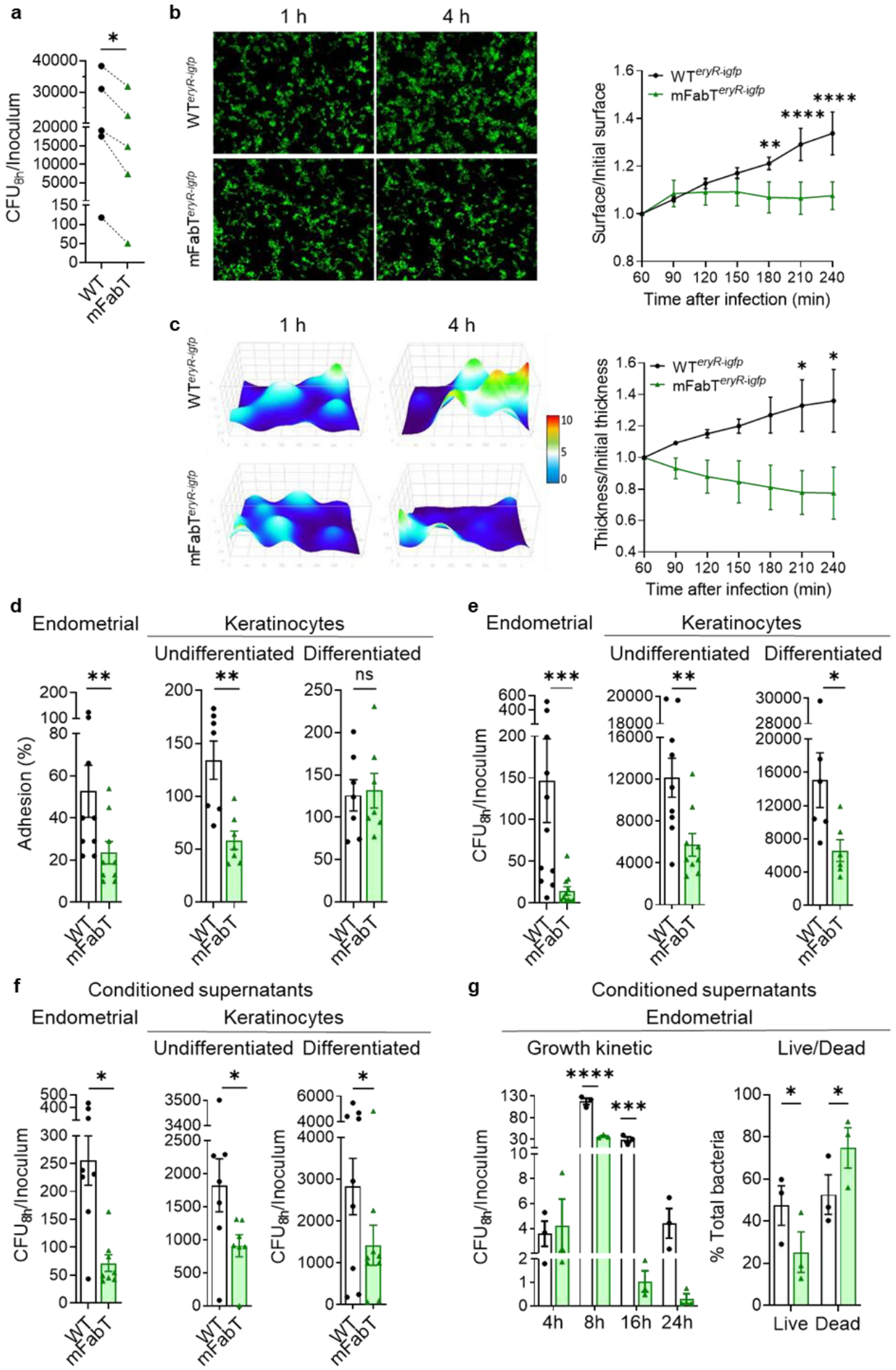
a
b
1 h
4 h
WTeryR-igfp
mFabTeryR-igfp
CFU8h/Inoculum
WT
mFabT
Surface/Initial surface
Time after infection (min)
c
Thickness/Initial thickness
d
Endometrial
Keratinocytes
Undifferentiated
Differentiated
Adhesion (%)
ns
e
f
Conditioned supernatants
g
Growth kinetic
Live/Dead
% Total bacteria
4h
8h
16h
24h
Live
Dead

Fig. 3

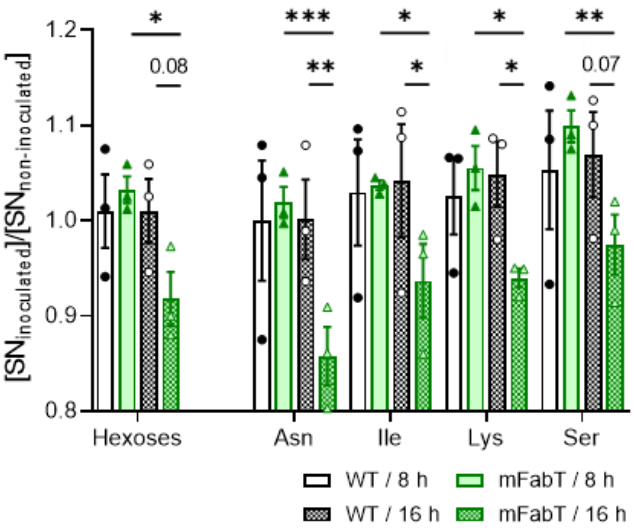
[SN_inoculated]/[SN_non-inoculated]
1.2
1.1
1.0
0.9
0.8
*
0.08
***
**
*
*
*
*
**
0.07
Hexoses
Asn
Ile
Lys
Ser
WT / 8 h
mFabT / 8 h
WT / 16 h
mFabT / 16 h

Fig. 4

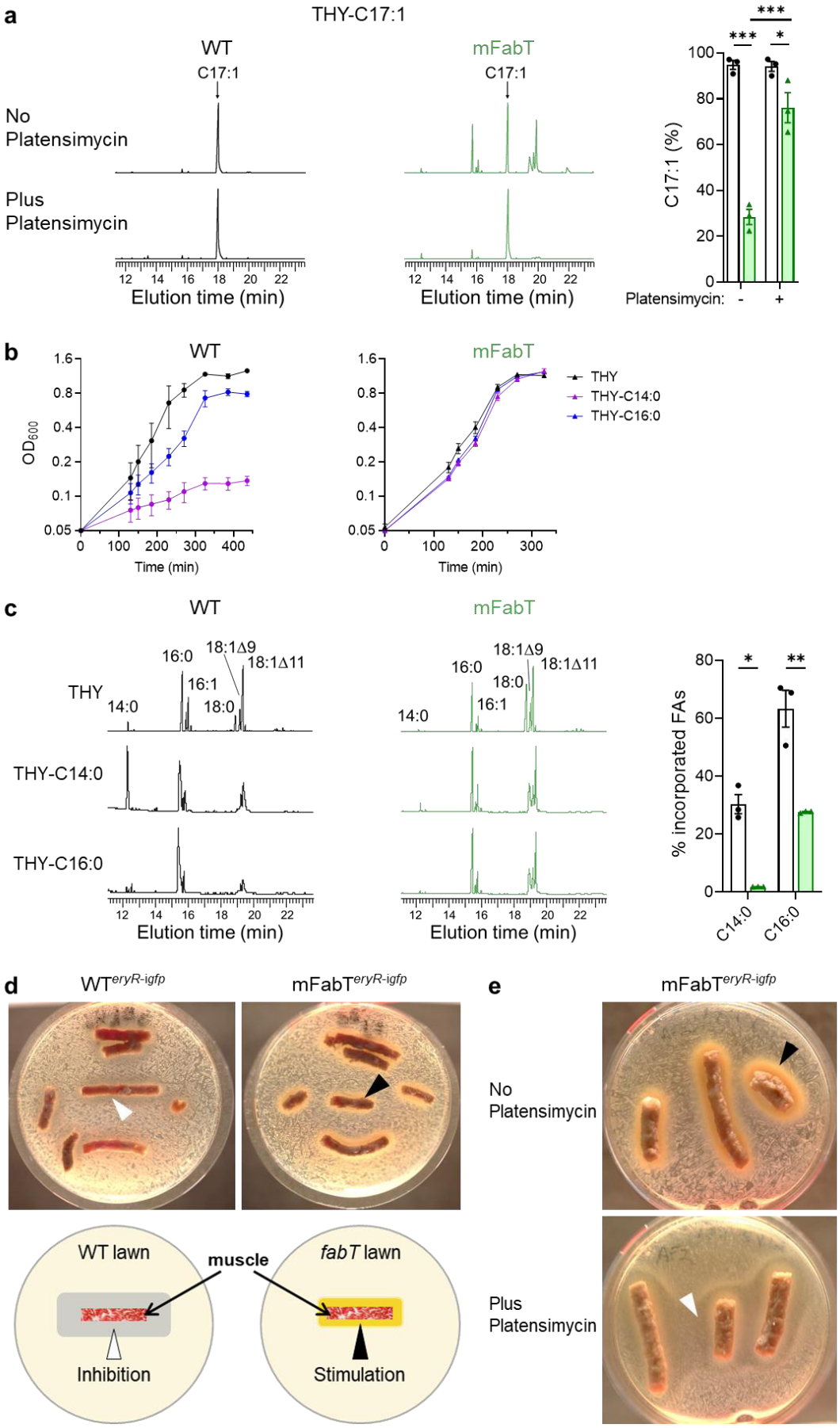
a
THY-C17:1
WT
mFabT
C17:1
No Platensimycin
Plus Platensimycin
Elution time (min)
C17:1 (%)
Platensimycin: - +
b
WT
mFabT
OD600
Time (min)
THY
THY-C14:0
THY-C16:0
c
WT
mFabT
THY
THY-C14:0
THY-C16:0
14:0
16:0
16:1
18:0
18:1Δ9
18:1Δ11
Elution time (min)
% incorporated FAs
C14:0
C16:0
d
WTeryR-igfp
mFabTeryR-igfp
WT lawn
muscle
fabT lawn
Inhibition
Stimulation
e
mFabTeryR-igfp
No Platensimycin
Plus Platensimycin

Fig. 5

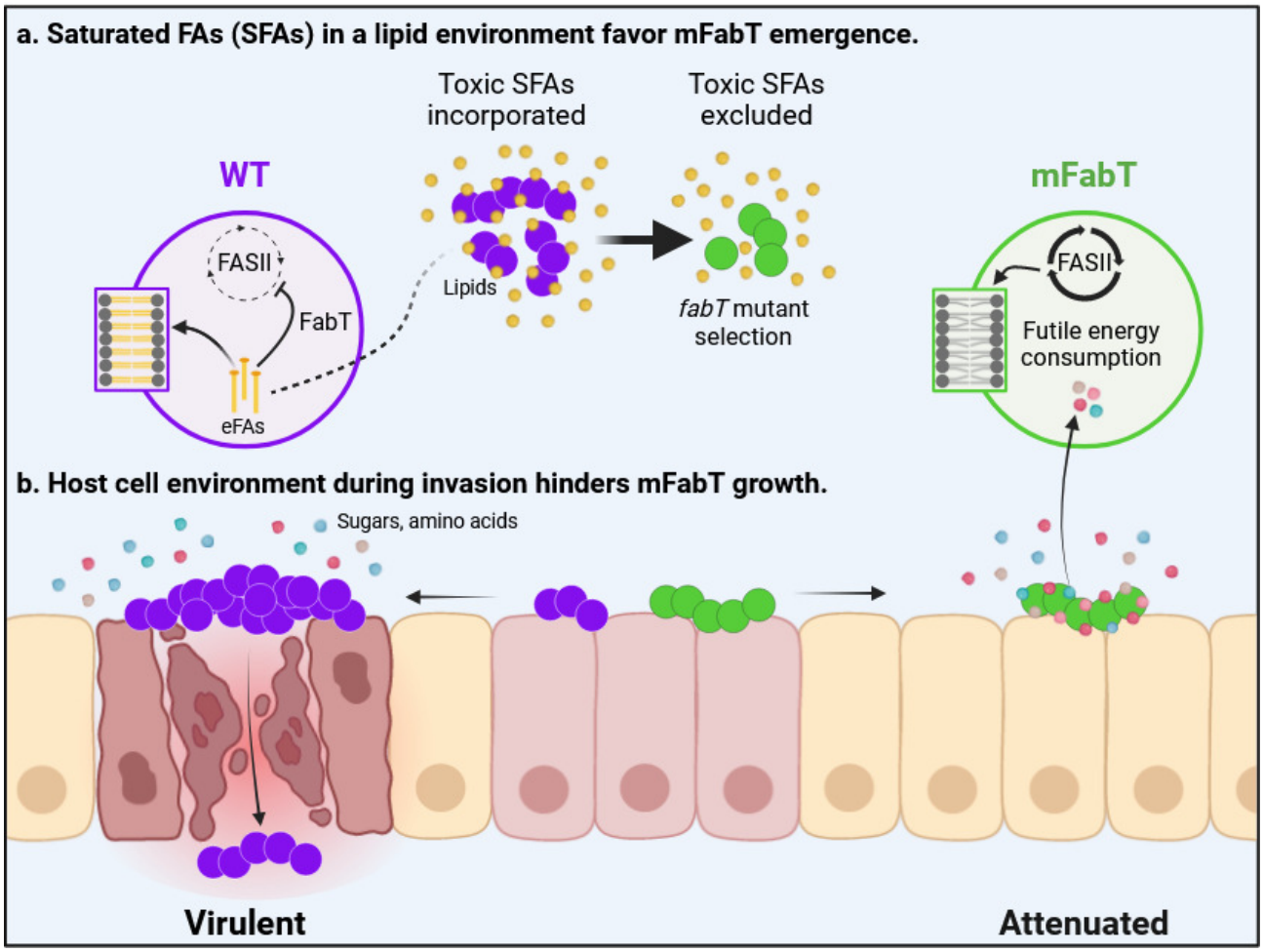
a. Saturated FAs (SFAs) in a lipid environment favor mFabT emergence.
Toxic SFAs incorporated
Toxic SFAs excluded
WT
mFabT
FASII
FabT
eFAs
Lipids
fabT mutant selection
FASII
Futile energy consumption
b. Host cell environment during invasion hinders mFabT growth.
Sugars, amino acids
Virulent
Attenuated

Fig. 6